Measurement of the beam-recoil polarization in low-energy virtual Compton scattering from the proton

(A1 Collaboration) Doria, L.; ...; Bosnar, Damir; ...; Makek, Mihael; ...; Weinriefer, M.

Source / Izvornik: **Physical Review C - Nuclear Physics, 2015, 92**

Journal article, Published version
Rad u časopisu, Objavljena verzija rada (izdavačev PDF)

https://doi.org/10.1103/PhysRevC.92.054307

Permanent link / Trajna poveznica: https://urn.nsk.hr/urn:nbn:hr:217:282164

Measurement of the beam-recoil polarization in low-energy virtual Compton scattering from the proton

L. Doria,[1,*] P. Janssens,[2] P. Achenbach,[1] C. Ayerbe Gayoso,[1] D. Baumann,[1] I. Bensafa,[3] M. Benali,[3] J. Beričič,[4] J. C. Bernauer,[1] R. Böhm,[1] D. Bosnar,[5] L. Correa,[3] N. D'Hose,[6] X. Defaÿ,[3] M. Ding,[1] M. O. Distler,[1] H. Fonvieille,[3] J. Friedrich,[1] J. M. Friedrich,[7] G. Laveissière,[3] M. Makek,[5] J. Marroncle,[6] H. Merkel,[1,†] M. Mihovilovič,[1] U. Müller,[1] L. Nungesser,[1] B. Pasquini,[8] J. Pochodzalla,[1] O. Postavaru,[1,9] M. Potokar,[4] D. Ryckbosch,[2] S. Sánchez Majos,[1] B. S. Schlimme,[1] M. Seimetz,[1] S. Širca,[4,10] G. Tamas,[1] R. Van de Vyver,[2] L. Van Hoorebeke,[2] A. Van Overloop,[2] Th. Walcher,[1] and M. Weinriefer[1]

(A1 Collaboration)

[1]*Institut für Kernphysik, Johannes Gutenberg–Universität Mainz, D-55099 Mainz, Germany*

[2]*Department of Physics and Astronomy, University of Gent, B-9000 Gent, Belgium*

[3]*Clermont Université, Université Blaise Pascal, CNRS/IN2P3, LPC, BP 10448, F-63000 Clermont-Ferrand, France*

[4]*Jožef Stefan Institute, SI-1000 Ljubljana, Slovenia*

[5]*Department of Physics, University of Zagreb, SI-10002 Zagreb, Croatia*

[6]*CEA IRFU/SPhN Saclay, F-91191 Gif-sur-Yvette Cedex, France*

[7]*Physik-Department, Technische Universität München, D-85748 Garching, Germany*

[8]*Dipartimento di Fisica, Universitá degli Studi di Pavia and INFN, I-27100 Pavia, Italy*

[9]*Institute of Space Science, RO 76900, Bucharest-Magurele, Romania*

[10]*Department of Physics, University of Ljubljana, SI-1000 Ljubljana, Slovenia*

(Received 22 May 2015; published 16 November 2015)

Double-polarization observables in the reaction $\vec{e}p \to e'\vec{p}\,'\gamma$ have been measured at $Q^2 = 0.33$ (GeV/c)^2. The experiment was performed at the spectrometer setup of the A1 Collaboration using the 855 MeV polarized electron beam provided by the Mainz Microtron (MAMI) and a recoil proton polarimeter. From the double-polarization observables the structure function $P_{LT}^{\perp}$ is extracted for the first time, with the value $(-15.4 \pm 3.3_{(\text{stat.})}\,^{+1.5}_{-2.4\ (\text{syst.})})$ GeV^{-2}, using the low-energy theorem for virtual Compton scattering. This structure function provides a hitherto unmeasured linear combination of the generalized polarizabilities of the proton.

DOI: 10.1103/PhysRevC.92.054307 PACS number(s): 13.60.Fz, 14.20.Dh, 25.30.Rw

I. INTRODUCTION

Polarizabilities parametrize the response of systems composed of charged constituents to electric and magnetic external fields. For the proton they contain information about the QCD interaction in the very low momentum-transfer domain where the coupling constant α_{strong} diverges. Since no static field of sufficient strength can be produced experimentally, they are measured by means of real Compton scattering (RCS). Now, due to the availability of powerful electron accelerators, also virtual Compton scattering (VCS) can be investigated. VCS allows for the determination of generalized polarizabilities (GPs) as function of the initial photon virtuality Q^2, as first pointed out in [1] for atomic nuclei and in [2] for nucleons. Just as the form factors G_E and G_M give access to the spatial density of charge and magnetization in the nucleon, the GPs give access to such densities for a nucleon deformed by an applied quasistatic electromagnetic field [2–5]. Out of the six lowest-order GPs of the proton, the electric and magnetic GPs have already been the subject of experimental investigation at MAMI [6,7], Bates [8], and JLab [9]. The four remaining ones, called the spin GPs, are still totally unknown experimentally. This paper presents the first measurement of a double-polarization observable in VCS, with the aim of gaining insight into the spin-GP sector of the nucleon for the first time.

II. FORMALISM AND NOTATION

VCS is experimentally accessed through the photon electroproduction reaction $ep \to e'p'\gamma$. At low energy it can be decomposed into a dominant Bethe-Heitler (BH) part, a VCS Born (B) part, and a VCS non-Born (nB) part, as shown in Fig. 1. The contributions of the Bethe-Heitler and Born processes (BH+B) can be exactly calculated using as input only the form factors of the nucleon. The non-Born part is parametrized at the first order in the real photon momentum q' by six GPs. With an unpolarized cross section measurement only two linear combinations of the GPs can be determined. To extract all the GPs, double-polarization measurements are required. In this experiment, the beam-recoil polarization asymmetries were measured in the reaction $\vec{e}p \to e'\vec{p}\,'\gamma$.

The main kinematical variables are defined in the (γp) center of mass (c.m.): the modulus of the momentum of the virtual photon $q_{\text{c.m.}}$, of the outgoing photon $q'_{\text{c.m.}}$, and the polar angle $\theta_{\gamma\gamma}$ between the two photons. The virtual photon polarization ϵ and the angle φ between the leptonic and reaction planes complete the kinematics.

The low-energy theorem (LET) for the double-polarization observables was developed in [3,10] and is only briefly recalled

*Now at TRIUMF, Vancouver, BC V6T 2A3, Canada.

†merkel@kph.uni-mainz.de

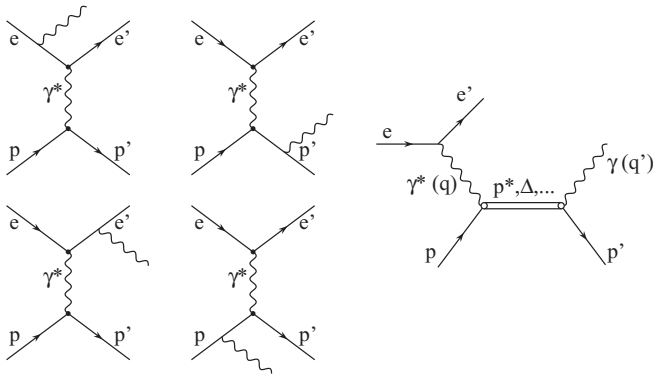

FIG. 1. Contributions to the photon electroproduction amplitude. The VCS non-Born contribution is parametrized by the GPs, while the BH+VCS Born contribution (BH+B) contains no GP effect and is entirely calculable in QED.

here. The double-polarization observable can be calculated via

$$\mathcal{P}_{\hat{\imath}}^{\text{c.m.}} = \frac{d^5\sigma(h,\hat{\imath}) - d^5\sigma(h,-\hat{\imath})}{d^5\sigma(h,\hat{\imath}) + d^5\sigma(h,-\hat{\imath})}, \tag{1}$$

where $\hat{\imath} = x,\ y,\ z$ is the c.m. axis for the recoil proton polarization component, $h = \pm\frac{1}{2}$ the beam helicity, and $d^5\sigma(h,\hat{\imath})$ the doubly polarized $(\vec{e}p \to e'\vec{p}\,'\gamma)$ cross section. The LET expansion, which is valid below pion threshold, leads to

$$\mathcal{P}_{\hat{\imath}}^{\text{c.m.}} = \frac{\Delta d^5\sigma^{\text{BH+B}} + \phi q'_{\text{c.m.}}\,\Delta\mathcal{M}^{\text{nB}}(h,\hat{\imath}) + O\left(q'^{\,2}_{\text{c.m.}}\right)}{2d^5\sigma}, \tag{2}$$

where $\Delta d^5\sigma^{\text{BH+B}}$ is the difference of the doubly polarized cross sections $d^5\sigma^{\text{BH+B}}(h,\hat{\imath}) - d^5\sigma^{\text{BH+B}}(h,-\hat{\imath})$ and $d^5\sigma$ is the unpolarized $(ep \to e'p'\gamma)$ cross section. $(\phi q'_{\text{c.m.}})$ is a phase-space factor. The non-Born terms $\Delta\mathcal{M}^{\text{nB}}$ are linear combinations of the VCS structure functions $P_{LT}^{\perp}$, $P_{TT}^{\perp}$, $P_{TT}^{\prime\perp}$, $P_{LT}^{\prime\perp}$, P_{LT}^{z}, $P_{LT}^{\prime z}$, which can be expressed as linear combinations of the six GPs. In particular, $P_{LT}^{\perp}$ is a linear combination of the structure functions P_{LL} and P_{TT}, where P_{LL} is proportional to the electric GP and P_{TT} is a combination of two spin GPs: $P^{(M1,M1)1}$ and $P^{(L1,M2)1}$, the latter corresponding to γ_{E1M2} in the RCS limit of $Q^2 \to 0$. For more detailed formulas, we refer the reader to Refs. [3,10].

III. EXPERIMENT

The experiment was performed at the spectrometer setup of the A1 Collaboration at MAMI [11], and details of the analysis can be found in [12,13]. Table I summarizes the two kinematical setups of the experiment.

The polarized electron beam was delivered by MAMI with an electron energy of $E = 854.6$ MeV and a longitudinal beam polarization of $P_b = 70\%$ on average. The beam polarization was determined by a Møller polarimeter and was flipped on a random basis with 1 Hz on average to avoid false asymmetries. A beam current of 22 μA was directed on a liquid hydrogen target with a length of 5 cm. The beam was rastered across the target to avoid local boiling.

TABLE I. Parameters of the spectrometer setups: p is the central momentum and θ the in-plane angle. Both settings are centered on the nominal kinematics defined by $q_{\text{c.m.}} = 600$ MeV/c, $\epsilon = 0.64$, $q'_{\text{c.m.}} = 90$ MeV/c and $\varphi = 180^\circ$. They differ in the covered in-plane c.m. angle $\theta_{\gamma\gamma}$.

Setup	Beam	Spectrometer A		Spectrometer B	
	E (MeV)	p_{proton} (MeV/c)	θ_{proton}	p_{electron} (MeV/c)	θ_{electron}
VCS90a	855	620	34.1°	546	50.6°
VCS90b	855	645	38.0°	539	50.6°

Two particles were detected in coincidence: the scattered electron in spectrometer B with a solid angle of 5.6 msr and a momentum resolution of 10^{-4}, and the recoil proton in spectrometer A with a solid angle of 21 msr and the same momentum resolution. Thanks to the good timing resolution of 0.9 ns (FWHM) for the coincidence time, no further particle identification was necessary. Behind the focal plane of spectrometer A, a proton polarimeter determined the transverse components of the proton polarization in the focal plane (see Refs. [14,15]).

The reaction was further identified by the missing mass squared, i.e., the squared mass M_X^2 of the missing particle X in the $(ep \to e'p'X)$ process. The M_X^2 distribution shows a clean peak at zero from photon electroproduction, which is well separated from the pion peak from π^0 electroproduction.

For the analysis, events with a missing mass squared of $-1000 < M_X^2 < 4000$ MeV$^2/c^4$ and a coincidence time of $-1.5 < t_{AB} < 1.5$ ns were accepted as VCS events. Events from the side bands of the coincidence time distribution were used to estimate the background contribution due to random coincidences. A cut was also required to eliminate the target endcaps.

For the determination of the polarization observables, only events below the pion threshold were selected, by a cut of $q'_{\text{c.m.}} < 126$ MeV/c. A standard set of further cuts were applied to ensure a clean reconstruction within the acceptance of the recoil polarimeter and to select the region of large analyzing power of the polarimeter [12]. A sample of about 77 000 VCS events survived the cuts.

IV. BEAM-RECOIL POLARIZATION ANALYSIS

With the polarimeter, for each event the direction of the secondary scattering process in the carbon analyzer was determined. This direction is given by the polar and azimuthal scattering angles Θ_s and Φ_s. The distribution of events is given by

$$\sigma(\Theta_s,\Phi_s,E_p) = \sigma_0\big[1 + A_C(\Theta_s,E_p)\mathcal{P}_y^{\text{fp}}\cos\Phi_s - A_C(\Theta_s,E_p)\mathcal{P}_x^{\text{fp}}\sin\Phi_s\big]; \tag{3}$$

it depends on the known analyzing power of the carbon analyzer $A_C(\Theta_s,E_p)$ (see [12,14]). The transverse components of the proton polarization in the focal plane is related to the double polarization observables by $\mathcal{P}_{x,y}^{\text{fp}} = 2\,h\,P_b\,P_{x,y}^{\text{fp}}$.

TABLE II. Results for the double-polarization observables. $P_x^{\text{c.m.}}$(raw) and $P_x^{\text{c.m.}}$(proj.) are the fitted $P_x^{\text{c.m.}}$ component before and after the projection to the nominal kinematics, respectively. $\Delta P_x^{\text{c.m.}}$(stat.) is the statistical error on $P_x^{\text{c.m.}}$(proj.), while $\Delta P_x^{\text{c.m.}}$(syst.) are systematic errors (see text). Negative $\theta_{\gamma\gamma}$ values are conventional for $\varphi = 180^\circ$.

$\theta_{\gamma\gamma}$		-170°	-150°	-130°	-110°	-90°
$P_y^{\text{c.m.}}$	(raw)	0.047	0.012	−0.043	0.020	−0.020
$\Delta P_y^{\text{c.m.}}$	(stat.)	±0.066	±0.053	±0.038	±0.041	±0.050
$P_x^{\text{c.m.}}$	(raw)	−0.220	−0.269	−0.215	−0.177	−0.067
$P_x^{\text{c.m.}}$	(proj.)	−0.209	−0.257	−0.201	−0.142	−0.041
$\Delta P_x^{\text{c.m.}}$	(stat.)	±0.049	±0.040	±0.030	±0.027	±0.027
$\Delta P_x^{\text{c.m.}}$	(syst.1)	±0.001	±0.011	±0.007	±0.009	±0.004
$\Delta P_x^{\text{c.m.}}$	(syst.2)	±0.030	±0.001	±0.003	±0.020	±0.030
$\Delta P_x^{\text{c.m.}}$	(syst.3)	±0.010	±0.020	±0.020	±0.020	±0.010

For a given set of c.m. polarizations $P_{x,y,z}^{\text{c.m.}}$, the focal plane transverse components P_x^{fp} and P_y^{fp} can be calculated by Lorentz transformation, rotation, and ray-tracing of the spin precession in the magnetic field of the spectrometer. Thus, the c.m. polarizations can be fitted to the distribution of the azimuthal angle Φ_s by a standard maximum likelihood method. This is the first step of the analysis.

In principle, the statistical ensemble contains the information for all three c.m. components of the polarization, since events with different orientation of the scattering plane have different paths in the magnetic field of the spectrometer, resulting in different transverse components in the focal plane. A detailed simulation showed, however, that the longitudinal component $P_z^{\text{c.m.}}$ cannot be reconstructed with sufficient resolution. Therefore this component was fixed in the analysis for each event to the value given by the BH+B calculation, i.e., $P_z^{\text{c.m.}} = \Delta d^5\sigma^{\text{BH+B}}/2d^5\sigma^{\text{BH+B}}$. The simulation showed that this choice was sufficient to provide a nonbiased fit of $P_y^{\text{c.m.}}$ and $P_x^{\text{c.m.}}$. A more realistic choice, i.e., adding a GP effect in the constraint on $P_z^{\text{c.m.}}$, was considered only to evaluate systematic errors.

The maximum likelihood fit yields the c.m. polarization components $P_x^{\text{c.m.}}$ and $P_y^{\text{c.m.}}$. The fit is made separately in five $\theta_{\gamma\gamma}$ bins to have sufficient statistical significance per bin.

Table II summarizes the results. The obtained values for $P_y^{\text{c.m.}}$ are compatible with zero within the uncertainties; this is consistent with the requirement that $P_y^{\text{c.m.}}$ has to vanish in strict in-plane kinematics. Globally, $P_y^{\text{c.m.}}$ has a negligible sensitivity to the GPs, and almost all the new information is carried by $P_x^{\text{c.m.}}$ through the term $\Delta\mathcal{M}^{\text{nB}}(h,\hat{x})$, which is of the form

$$\Delta\mathcal{M}^{\text{nB}}(h,\hat{x}) = h\left(a_1^x P_{LT}^{\perp} + a_2^x P_{TT}^{\perp} + a_3^x P_{TT}^{\prime\perp} + a_4^x P_{LT}^{\prime\perp}\right), \quad (4)$$

with a_i^x being known kinematical coefficients [10].

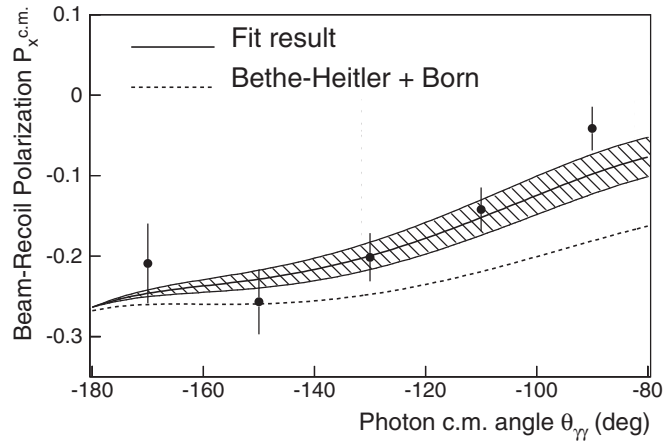

FIG. 2. Measured recoil proton polarization component $P_x^{\text{c.m.}}$ in the c.m. frame. The five points with their statistical error are the result of the first-step fit. The solid curve is calculated using our result for $P_{LT}^{\perp}$ (see text); the shaded band represents the statistical uncertainty. The dashed curve is the BH+B calculation of $P_x^{\text{c.m.}}$, i.e., without any GP effect.

Figure 2 displays the measured $P_x^{\text{c.m.}}$ component as five solid points. These points have been projected to the nominal kinematics ($q_{\text{c.m.}}$, ϵ, $q'_{\text{c.m.}}$, and φ of Table I), completed by the values of $\theta_{\gamma\gamma}$ of Table II. This projection is based on the expected LET behavior of the polarization observables as a function of the kinematics.

The statistical error is provided by the fit. Systematic errors on $P_x^{\text{c.m.}}$ have been determined as coming from (1) a beam polarization uncertainty of ± 1.2%, (2) changing the constraint on $P_z^{\text{c.m.}}$, and (3) uncertainties in the kinematical projection. Other systematic effects, due to instrumental asymmetries in the proton polarimeter or due to random coincidences under the time peak, were found to be negligible.

V. STRUCTURE FUNCTION ANALYSIS

As a next step, a fit was performed with the aim of determining individual GPs (including the spin GPs). The

TABLE III. The complete set of VCS structure functions at $Q^2 = 0.33$ (GeV/c)^2 as calculated by two models: (I) DR formalism [16] (with $\Lambda_\alpha = 1.80$ GeV, $\Lambda_\beta = 0.75$ GeV and the MAID03 version); (II) HBChPT at $O(p^3)$ [17], including the π^0-pole term (or anomaly). Only six of these nine structure functions are independent, e.g., the ones in the first six columns. $P_{TT}^{\perp}$, $P_{TT}^{\prime\perp}$, and $P_{LT}^{\prime\perp}$ are fixed to the values of this table when fitting $P_{LT}^{\perp}$ (see text). All calculations are done with the proton form factors of Ref. [18]. This also holds for Table V.

	Model Structure functions (GeV^{-2})								
Model	$P_{TT}^{\perp}$	$P_{TT}^{\prime\perp}$	$P_{LT}^{\perp}$	$P_{LT}^{\prime\perp}$	P_{LT}	P_{LL}	P_{TT}	P_{LT}^{z}	$P_{LT}^{\prime z}$
(I) DR model	0.97	−0.44	−10.83	−1.43	−2.43	22.40	−1.58	−1.34	−1.21
(II) HBChPT $\mathcal{O}(p^3)$	2.05	0.62	−10.57	−4.21	−5.34	15.07	−6.89	−3.03	−0.86

principle is again to use the likelihood method, this time fully unbinned. The non-Born terms $\Delta\mathcal{M}^{\rm nB}(h,\hat{x})$ and $\Delta\mathcal{M}^{\rm nB}(h,\hat{y})$ in the numerator of $P_x^{\rm c.m.}$ and $P_y^{\rm c.m.}$ were replaced by their analytical expression in terms of the GPs [10]. The cross section $d^5\sigma$ in the denominator of $P_x^{\rm c.m.}$ and $P_y^{\rm c.m.}$ was fixed to its value given by the unpolarized LET expression, using our previously measured structure functions $(P_{LL} - P_{TT}/\epsilon)$ and P_{LT} [7]. As an outcome, it turned out that the data were not precise enough to extract individual GPs. However, if one uses structure functions, i.e., combinations of GPs, instead of GPs directly, one gets a significant result for $P_{LT}^{\perp}$ as we show in the following final step of the analysis.

The unbinned maximum likelihood method is again used. The non-Born terms $\Delta\mathcal{M}^{\rm nB}(h,\hat{x})$ and $\Delta\mathcal{M}^{\rm nB}(h,\hat{y})$ are replaced by their analytical expressions in terms of the structure functions, as in Eq. (4), for example. The denominators of $P_x^{\rm c.m.}$ and $P_y^{\rm c.m.}$ are treated as above.

Exploratory fits showed that $\Delta\mathcal{M}^{\rm nB}$ is sensitive mainly to $P_{LT}^{\perp}$, among the four structure functions entering Eq. (4). Therefore, the other three, $P_{TT}^{\perp}, P_{TT}^{\prime\perp}$, and $P_{LT}^{\prime\perp}$, cannot be fitted. However, their influence can be investigated by inserting several model predictions and fitting $P_{LT}^{\perp}$ only. This implies a model dependence of the extracted results, but we show in the following that it is relatively small compared to the statistical uncertainty.

The structure functions that need to be fixed are only $P_{TT}^{\perp}$, $P_{TT}^{\prime\perp}$, and $P_{LT}^{\prime\perp}$, i.e., the ones appearing in $\Delta\mathcal{M}^{\rm nB}(h,\hat{x})$ and $\Delta\mathcal{M}^{\rm nB}(h,\hat{y})$, except $P_{LT}^{\perp}$. The maximum likelihood fit was done with three rather different assumptions for these fixed structure functions. In fit "I" they were set to values calculated by the dispersion relation (DR) model [16]; cf. the first line of Table III. In fit "II" they were set to values calculated by heavy baryon chiral perturbation theory (HBChPT) [17]; cf. the second line of Table III. In fit "III" they were all set to zero. These different choices lead to the following results: $P_{LT}^{\perp} = -15.4, -17.7$ and -14.1 GeV^{-2} for fits "I", "II", and "III" respectively. We consider fit "I" as the central one, yielding our final result for $P_{LT}^{\perp}$, and the two other results are used to estimate the model-dependent error.

The statistical error on $P_{LT}^{\perp}$ is provided by the maximum likelihood fit. The systematic error comes from several main sources, which are estimated in Table IV. The first contribution is obtained by changing the beam polarization by $\pm$ 1.2% in the analysis. The second contribution is estimated by performing the fit with several form factor parametrizations [19–22]; the maximal spread of the results gives the magnitude of the error, which remains small. The third contribution is related to the treatment of $P_z^{\rm c.m.}$; the error is obtained as the difference in the fitted result when we fix $P_z^{\rm c.m.}$ to its BH+B value, or when a GP effect is added to it. The fourth contribution is due to model dependence; it is determined from the differences between the various fits ("II" − "I" and "III" − "I"). In Table IV each partial systematic error has been symmetrized except the fourth one which is the largest and most asymmetric. The total systematic error is calculated as the quadratic sum of the errors of Table IV for each sign separately.

TABLE IV. Systematic errors in the extraction of $P_{LT}^{\perp}$.

Error type	Error value (GeV^{-2})
Beam polarization ($\pm$1.2%)	$\mp$ 0.53
Proton form factors	$\pm$ 0.10
Constraint on $P_z^{\rm c.m.}$	$\pm$ 0.47
Fixed structure functions	$+1.26/-2.29$
Total systematic error	$+1.45/-2.40$

TABLE V. Our measured value of $P_{LT}^{\perp}$ and several model predictions at $Q^2 = 0.33$ (GeV/c)^2. For the DR model, the (a), (b), and (c) cases correspond to different values of the Λ_α parameter: 0.6, 1.2, and 1.8 GeV respectively (see text).

	$P_{LT}^{\perp}$ (GeV^{-2})
This experiment	$-15.4 \pm 3.3_{\rm (stat.)}\,^{+1.5}_{-2.4\ \rm (syst.)}$
DR model [16]	-3.7 (a), -8.7 (b), -10.8 (c)
HBChPT $O(p^3)$ [17]	-10.6

Our final result for $P_{LT}^{\perp}$ is presented in Table V. It is compared to theoretical values from HBChPT and DR calculations. The absolute value of the result is larger than in most theoretical calculations. Some features of the models are worth noting: In HBChPT some of the GPs have a bad convergence with respect to the order of the calculation [23,24], and this may affect the model value of $P_{LT}^{\perp}$. In the DR model the spin GPs are entirely fixed, but the scalar GPs contain an unconstrained part that has to be fitted from experiment. In particular $P_{LT}^{\perp}$ depends, via the structure function P_{LL}, on the free parameter Λ_α which determines the electric GP. Table V shows this dependence for a realistic range of values for Λ_α. We note that the DR model has a lower limit for $P_{LT}^{\perp}$ of -13.1 GeV^{-2} (for $\Lambda_\alpha = \infty$).

A graphical representation of our result is shown in Fig. 2. The central solid curve is obtained by calculating the polarization component $P_x^{\rm c.m.}$ at the nominal kinematics, based on Eqs. (2) and (4). The calculation uses the results of fit "I" (see above), i.e., $P_{LT}^{\perp} = -15.4$ GeV^{-2}, and the other three structure functions set to their DR value of Table III. Using the results of fit "II" instead of "I" yields a very similar curve. The deviation from the BH+B calculation (dashed curve) is a clear signature of the polarizability effect.

VI. CONCLUSIONS

In conclusion, we have measured for the first time double-polarization observables in VCS from the proton below the pion threshold. The analysis was based on the theoretical formulation of the LET for polarized VCS, and the experimental use of recoil proton polarimetry. A clear polarizability effect was observed in the $P_x^{\rm c.m.}$ polarization component. We extracted one new structure function, $P_{LT}^{\perp}$, and found a value that is larger in magnitude than most theoretical calculations. Therefore, this measurement provides a valuable and entirely new constraint for models of nucleon structure, although it does not allow one to further disentangle the scalar and spin GPs of the proton.

ACKNOWLEDGMENTS

We acknowledge the MAMI accelerator group for outstanding support. This work was supported in part by the FWO-Flanders (Belgium), the BOF-Gent University, the Deutsche Forschungsgemeinschaft with the Collaborative Research Center 1044, the Federal State of Rhineland-Palatinate, the Croatian Science Foundation project HRZZ 1680, and the French CEA and CNRS/IN2P3. P.J. was supported by a fellowship from the Research Foundation–Flanders (FWO).

[1] H. Arenhövel and D. Drechsel, Nucl. Phys. A **233**, 152 (1974).
[2] P. A. M. Guichon, G. Q. Liu, and A. W. Thomas, Nucl. Phys. A **591**, 606 (1995).
[3] P. A. M. Guichon and M. Vanderhaeghen, Prog. Part. Nucl. Phys. **41**, 125 (1998).
[4] M. Gorchtein, C. Lorce, B. Pasquini, and M. Vanderhaeghen, Phys. Rev. Lett. **104**, 112001 (2010).
[5] B. R. Holstein and S. Scherer, Annu. Rev. Nucl. Part. Sci. **64**, 51 (2014).
[6] J. Roche *et al.*, Phys. Rev. Lett. **85**, 708 (2000).
[7] P. Janssens *et al.* (A1 Collaboration), Eur. Phys. J. A **37**, 1 (2008).
[8] P. Bourgeois, Y. Sato, J. Shaw, R. Alarcon, A. Bernstein *et al.*, Phys. Rev. C **84**, 035206 (2011).
[9] H. Fonvieille *et al.* (Jefferson Lab Hall A Collaboration), Phys. Rev. C **86**, 015210 (2012).
[10] M. Vanderhaeghen, Phys. Lett. B **402**, 243 (1997).
[11] K. I. Blomqvist *et al.*, Nucl. Instrum. Methods A **403**, 263 (1998).
[12] L. Doria, Ph.D. thesis, Johannes Gutenberg-Universität Mainz, Germany, 2008 (unpublished).
[13] P. Janssens, Ph.D. thesis, Gent University, Belgium, 2007 (unpublished).
[14] T. Pospischil *et al.*, Nucl. Instrum. Methods A **483**, 713 (2002).
[15] T. Pospischil *et al.*, Nucl. Instrum. Methods A **483**, 726 (2002).
[16] B. Pasquini *et al.*, Eur. Phys. J. A **11**, 185 (2001).
[17] T. R. Hemmert, B. R. Holstein, G. Knochlein, and D. Drechsel, Phys. Rev. D **62**, 014013 (2000).
[18] P. Mergell, U. G. Meissner, and D. Drechsel, Nucl. Phys. A **596**, 367 (1996).
[19] J. Arrington, W. Melnitchouk, and J. A. Tjon, Phys. Rev. C **76**, 035205 (2007).
[20] J. Friedrich and T. Walcher, Eur. Phys. J. A **17**, 607 (2003).
[21] M. A. Belushkin, H.-W. Hammer, and Ulf-G. Meissner, Phys. Rev. C **75**, 035202 (2007).
[22] J. C. Bernauer *et al.* (A1 Collaboration), Phys. Rev. C **90**, 015206 (2014).
[23] C.-W. Kao and M. Vanderhaeghen, Phys. Rev. Lett. **89**, 272002 (2002).
[24] C.-W. Kao, B. Pasquini, and M. Vanderhaeghen, Phys. Rev. D **70**, 114004 (2004).